Pergamon

Int. J. Heat Mass Transfer. Vol. 38, No. 7, pp. 1297–1303, 1995

0017-9310/95 $9.50+0.00

0017-9310(94)00239-8

The influence of an impermeable surface on pore steam pressure during drying of refractory concrete slabs

ZHEN-XIANG GONG and ARUN S. MUJUMDAR
Department of Chemical Engineering, McGill University, Montreal, Quebec, Canada H3A 2A7

(*Received* 4 *May* 1994 *and in final form* 18 *July* 1994)

Abstract—A finite-element model is developed for the heat and mass transfer process in refractory concrete. Using this model, simulations are carried out for drying of refractory concrete slabs heated on one side only to investigate the effects of an impermeable surface, which may be either the heated face or the unheated face, on pore steam pressure and moisture removal rate. Simulation results indicate that the presence of an impermeable surface produces a very significant rise of pore steam pressure which may result in explosive spalling of the concrete.

INTRODUCTION

Refractory concrete is used to build high-temperature installations such as those encountered, for example, in the iron and steel industry. After curing, refractory concrete castables still contain a large amount of water. They must be carefully dried before putting them into service to avoid inferior quality and even destruction by explosive spalling resulting from rapid heating when exposed to elevated temperatures.

In drying, thermal evaporation of the water within the pores leads to a rise in the steam pressure due to limited permeability of the concrete. This pore steam pressure is thought to be both the driving force for moisture transfer and the direct cause of explosive spalling. Therefore, prediction of the pore steam pressure is of practical importance to the drying of refractory concrete castables.

Based on a diffusion theory, Bazant and Thonguthai [1] developed a mathematical model to describe the heat and mass transfer process in refractory concrete. Bazant and Thonguthai [2] and Bazant *et al.* [3] solved this model by the finite-element method for failure analysis of concrete reactor vessels in accidents and concrete structures subjected to fire. Dhatt *et al.* [4] also utilized a finite-element model to calculate the temperature and pore steam pressure responses to various heating rates for a one-dimensional axisymmetric geometry. Gong *et al.* [5] developed a finite-element model to simulate the drying of refractory concrete by convection and volumetric heating. Gong *et al.* [6] also simulated the one-side heating drying of refractory concrete slabs and proposed a set of rules for drying schedules according to the thicknesses of refractory concrete. The first attempt to simulate the kiln-drying process of refractory concrete was carried out by Gong and Mujumdar [7]. They set up a one-dimensional finite element model and simulated different time–temperature schedules. Recently they extended their model to two dimensions [8].

Drying of refractory concrete is influenced by many factors. Among these are the thermal and mass transfer boundary conditions which have a direct effect on both moisture removal and pore steam pressure produced in the drying process. Creating an appropriate boundary condition can enhance the drying rate as well as quality of dry products. Boundary conditions are decided by both the drying operation and the manufacturing technologies. Therefore, a detailed understanding of the influence of the boundary conditions on the transport process is not only helpful to improve the drying operation, but also to provide guidance for improvement of the manufacturing technology.

In this paper, a finite-element model is described for drying of refractory concrete. Simulation results are obtained for one-side heating drying of refractory concrete slabs. The effects of an impermeable surface which may be either the heated one or the unheated one, on pore steam pressure and moisture removal rate are investigated and analyzed.

MATHEMATICAL MODEL

The governing equations of the heat and mass transfer process in refractory concrete according to the simplified model of Bazant and Thonguthai [1] are as follows:

$$\frac{\partial W}{\partial t}=\frac{\partial}{\partial x}\left(\frac{a}{g}\frac{\partial P}{\partial x}\right)+\frac{\partial}{\partial y}\left(\frac{a}{g}\frac{\partial P}{\partial y}\right)+\frac{\partial}{\partial z}\left(\frac{a}{g}\frac{\partial P}{\partial z}\right)+\frac{\partial W_{\mathrm{d}}}{\partial t} \quad (1)$$

NOMENCLATURE

a permeability [m s^{-1}]
a_0 permeability at reference temperature T_0 [m s^{-1}]
B_T convection heat transfer coefficient [W m^{-2} K^{-1}]
B_w convection mass transfer coefficient [s m^{-1}]
C specific heat of concrete [J kg^{-1} K^{-1}]
C_a evaporation heat of water [J kg^{-1}]
C_m submatrix ($m = 1, 2, 3, 4$)
C_w specific heat of water [J kg^{-1} K^{-1}]
F_1, F_2 subvectors
g gravity acceleration (9.806 m s^{-2})
h relative humidity in the pore, $h = P/P_s(T)$
k thermal conductivity of concrete [W m^{-1} K^{-1}]
K_1, K_2 submatrices
L thickness of concrete slab [m]
n outward normal of boundary
nel element number
nen node number of an element
N_I, N_J shape functions
P pore steam pressure [N m^{-2}]
P_{en} ambient steam partial pressure [N m^{-2}]
P_s saturation pressure of water [N m^{-2}]
P_w pressure at boundary [N m^{-2}]
t time [s]
T temperature [°C]
T_0 reference temperature [°C]
T_{en} ambient temperature [°C]
T_w boundary temperature [°C]
W free water content [kg m^{-3}]
W_0 saturation water content at reference temperature T_0 [kg m^{-3}]
W_1, W_2 free water content when $h = 0.96$ and 1.04, respectively [kg m^{-3}]
W_c anhydrous cement content per m^3 of concrete [kg m^{-3}]
W_d water liberated by dehydration during heating [kg m^{-3}]
x, y, z coordinates.

Greek symbols
Γ boundary surface
γ a time integral parameter, $\gamma = 0$–1
Δt time step [s]
ρ mass density [kg m^{-3}]
Ω solution domain.

Subscript
n the nth time step.

Superscripts
e element
i the ith iteration.

$$\rho C\frac{\partial T}{\partial t}-C_a\frac{\partial W}{\partial t}=-C_w\frac{a}{g}\left(\frac{\partial P}{\partial x}\frac{\partial T}{\partial x}+\frac{\partial P}{\partial y}\frac{\partial T}{\partial y}+\frac{\partial P}{\partial z}\frac{\partial T}{\partial z}\right)+\frac{\partial}{\partial x}\left(k\frac{\partial T}{\partial x}\right)+\frac{\partial}{\partial y}\left(k\frac{\partial T}{\partial y}\right)+\frac{\partial}{\partial z}\left(k\frac{\partial T}{\partial z}\right). \quad (2)$$

This model has been verified to be in agreement with experiments (see ref. [3]). So, it is suitable for the engineering application under study.

Since W is a function of temperature T and pore steam pressure P, $W = W(P, T)$, we can write

$$\frac{\partial W}{\partial t}=\frac{\partial W}{\partial P}\frac{\partial P}{\partial t}+\frac{\partial W}{\partial T}\frac{\partial T}{\partial t}. \quad (3)$$

Substitution of equation (3) into equations (1) and (2) yields

$$A_1\frac{\partial P}{\partial t}+A_3\frac{\partial T}{\partial t}=\frac{\partial}{\partial x}\left(\frac{a}{g}\frac{\partial P}{\partial x}\right)+\frac{\partial}{\partial y}\left(\frac{a}{g}\frac{\partial P}{\partial y}\right)+\frac{\partial}{\partial z}\left(\frac{a}{g}\frac{\partial P}{\partial z}\right)+\frac{\partial W_d}{\partial t} \quad (4)$$

$$A_2\frac{\partial P}{\partial t}+A_4\frac{\partial T}{\partial t}=-C_w\frac{a}{g}\left(\frac{\partial P}{\partial x}\frac{\partial T}{\partial x}+\frac{\partial P}{\partial y}\frac{\partial T}{\partial y}+\frac{\partial P}{\partial z}\frac{\partial T}{\partial z}\right)+\frac{\partial}{\partial x}\left(k\frac{\partial T}{\partial x}\right)+\frac{\partial}{\partial y}\left(k\frac{\partial T}{\partial y}\right)+\frac{\partial}{\partial z}\left(k\frac{\partial T}{\partial z}\right) \quad (5)$$

where

$$A_1=\frac{\partial W}{\partial P}\quad A_2=-C_a\frac{\partial W}{\partial P}\quad A_3=\frac{\partial W}{\partial T}\quad A_4=\rho C-C_a\frac{\partial W}{\partial T}. \quad (6)$$

The boundary conditions are:
for pressure

$$-\frac{a}{g}\frac{\partial P}{\partial n}=B_w(P-P_{en}) \quad (7)$$

$$P=P_w \quad (8)$$

and for temperature

$$-k\frac{\partial T}{\partial n}=B_T(T-T_{en})+C_aB_w(P-P_{en}) \quad (9)$$

$$T=T_w. \quad (10)$$

FINITE ELEMENT FORMULATION

After spacewise discretization of equations (4) and (5), subject to convective boundary conditions [equations (7) and (9)], is accomplished using Galerkin's method [9], the following semi-discrete matrix system is obtained:

$$[C]\{\dot{U}\}+[K]\{U\}=\{F\} \tag{11}$$

in which

$$[C]=\sum_{i=1}^{nel}\begin{bmatrix}C_1 & C_3\\ C_2 & C_4\end{bmatrix}^e \quad [K]=\sum_{i=1}^{nel}\begin{bmatrix}K_1 & 0\\ 0 & K_2\end{bmatrix}^e \tag{12}$$

and

$$\{U\}=\sum_{i=1}^{nel}\begin{Bmatrix}P\\ T\end{Bmatrix}^e \quad \{F\}=\sum_{i=1}^{nel}\begin{Bmatrix}F_1\\ F_2\end{Bmatrix}^e. \tag{13}$$

In the preceding equations, the superposed dot denotes differentiation with respect to time; C_m ($m=1, 2, 3, 4$), K_1 and K_2 are submatrices; F_1 and F_2 are subvectors. The coefficients in the submatrices and subvectors are calculated according to the following equations:

$$C_m^{IJ}=\int_{\Omega^e}A_mN_IN_J\,dx\,dy\,dz \tag{14}$$

$$K_1^{IJ}=\int_{\Omega^e}\frac{a}{g}\left(\frac{\partial N_I}{\partial x}\frac{\partial N_J}{\partial x}+\frac{\partial N_I}{\partial y}\frac{\partial N_J}{\partial y}+\frac{\partial N_I}{\partial z}\frac{\partial N_J}{\partial z}\right)dx\,dy\,dz+\int_{\Gamma^e}B_wN_IN_J\,d\Gamma \tag{15}$$

$$K_2^{IJ}=\int_{\Omega^e}\left[k\left(\frac{\partial N_I}{\partial x}\frac{\partial N_J}{\partial x}+\frac{\partial N_I}{\partial y}\frac{\partial N_J}{\partial y}+\frac{\partial N_I}{\partial z}\frac{\partial N_J}{\partial z}\right)+A_{vx}N_I\frac{\partial N_J}{\partial x}+A_{vy}N_I\frac{\partial N_J}{\partial y}+A_{vz}N_I\frac{\partial N_J}{\partial z}\right]dx\,dy\,dz+\int_{\Gamma^e}(B_TN_IN_J+C_aB_wN_IN_J)\,d\Gamma \tag{16}$$

$$F_1^I=\int_{\Omega^e}A_dN_I\,dx\,dy\,dz+\int_{\Gamma^e}B_wP_{en}N_I\,d\Gamma \tag{17}$$

$$F_2^I=\int_{\Gamma^e}(B_TT_{en}+C_aB_wP_{en})\,N_I\,d\Gamma \tag{18}$$

where

$$A_{vx}=\frac{a}{g}C_w\frac{\partial P}{\partial x}A_{vy}=\frac{a}{g}C_w\frac{\partial P}{\partial y}a_{vz}=\frac{a}{g}C_w\frac{\partial P}{\partial z} \tag{19}$$

$$A_d=\frac{\partial W_d}{\partial t}. \tag{20}$$

Discretization of the time derivatives in equation (11) is most often achieved with a finite difference technique. In this work, a predictor–corrector scheme [10] is adopted.

Predictors:

$$\{U_{n+1}^0\}=\{U_n\}+(1-\gamma)\Delta t\{\dot{U}_n\} \tag{21}$$

$$\{\dot{U}_{n+1}^0\}=\{0\}. \tag{22}$$

Correctors:

$$\{U_{n+1}^{i+1}\}=\{U_{n+1}^0\}+\gamma\Delta t\{\dot{U}_{n+1}^{i+1}\} \tag{23}$$

$$\{\dot{U}_{n+1}^{i+1}\}=\{\dot{U}_{n+1}^i\}+\{\Delta\dot{U}_{n+1}^i\}. \tag{24}$$

Substitution of equations (23) and (24) into equation (11) yields

$$[K^*]\{\Delta\dot{U}_{n+1}^i\}=\{R_{n+1}^i\} \tag{25}$$

where

$$[K^*]=[C(U_{n+1}^i)]+\gamma\Delta t[K(U_{n+1}^i)] \tag{26}$$

$$\{R(U_{n+1}^i)\}=\{F(U_{n+1}^i)\}-[K(U_{n+1}^i)]\{U_{n+1}^i\}-[C(U_{n+1}^i)]\{\dot{U}_{n+1}^i\}. \tag{27}$$

The solution procedure is as follows:

(1) At the beginning of each time step, calculate $\{U_{n+1}^0\}$ and $\{\dot{U}_{n+1}^0\}$ according to equations (21) and (22);

(2) With the two starting vectors, solve equation (25) for $\{\Delta\dot{U}_{n+1}^i\}$;

(3) Update $\{\dot{U}_{n+1}^{i+1}\}$ and $\{U_{n+1}^{i+1}\}$ using equations (24) and (23);

(4) If the convergence condition is met (here, we compare the Cartesian norms of $\{\Delta\dot{U}_{n+1}^i\}$ and $\{R\}$ with some selected constants TOL1 and TOL2), set

$$\{U_{n+1}\}=\{U_{n+1}^{i+1}\} \tag{28}$$

and

$$\{\dot{U}_{n+1}\}=\{\dot{U}_{n+1}^{i+1}\} \tag{29}$$

if not, using $\{U_{n+1}^{i+1}\}$ and $\{\dot{U}_{n+1}^{i+1}\}$ as starting vectors, go to step (2) and undertake the next iteration.

Based on the procedure described above, a finite element computer code for one-, two- and three-dimensional problems, called DRY-RC, has been developed with FORTRAN 77. Using this code, simulations are carried out for one-side heating drying of refractory concrete slabs. All the computations in this work are carried out in a 486 personal computer running at 25 MHz. The results were tested to be independent of mesh size.

RESULTS AND DISCUSSION

A refractory concrete slab of 200 mm thickness is used to model the influence of an impermeable surface which may be either the heated or the unheated one, on the development of pore steam pressure and moisture removal rates. Initially the refractory concrete slab is prescribed to have a uniform temperature of 25°C with a relative humidity of P/P_s (25°C) = 90% in the pore. When dried by one-side heating, the

Table 1. Computed cases

Case no.	Heated surface	Unheated surface	
	Mass boundary	Mass boundary	Thermal boundary
1	Impermeable	Permeable	Convection
2	Permeable	Impermeable	Convection
3	Permeable	Impermeable	Adiabatic
4	Permeable	Permeable	Convection

temperature of the heated surface is required to increase in accordance to a prescribed time–temperature schedule to ensure a good quality and possibly a shorter drying time.

To investigate the influence of an impermeable surface on the pore steam pressure and the moisture removal rate, four cases were computed as listed in Table 1.

When a surface is impermeable, the moisture flux at this surface is zero; while for an adiabatic surface, the heat flux is zero. In reality, the surface of a concrete installation cannot be completely impermeable. Assumption of a completely impermeable surface is made only to accentuate the effect of poor mass transfer at the boundary. When a surface is permeable, the moisture flux can be described by equation (7) and when there is convection heat transfer at the unheated surface, the heat flux can be described by equation (9).

The parameters used in the computations are listed in Table 2.

The permeability, a, is strongly dependent on both moisture and temperature. It is computed according to the following empirical correlation [1,2,11]:

$$a = \begin{cases} a_0 f_1(h,T) f_2(T) & (T \leqslant 95^\circ\text{C}) \\ 5.6\, a_0 f_3(T) & (T > 95^\circ\text{C}) \end{cases} \tag{30}$$

where

$$f_1(h,T) = \begin{cases} \dfrac{1.28929 - 0.013571T}{1+[4(1-h)]^4} + 0.013571T - 0.28929 & (h < 1) \\ 1 & (h \geqslant 1) \end{cases} \tag{31}$$

$$f_2(T) = \exp\left[2700\left(\frac{1}{273+T_0} - \frac{1}{273+T}\right)\right] \tag{32}$$

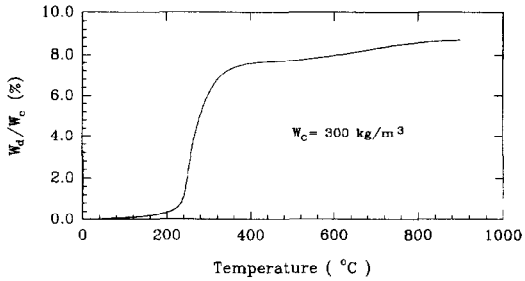

Fig. 1. Dehydration curve.

$$f_3(T) = \exp\left[\frac{T-95}{0.881+0.214(T-95)}\right]. \tag{33}$$

$\partial W/\partial P$ and $\partial W/\partial T$ are obtained from the following state equation, $W = W(P, T)$ [1,2,11]:

$$W = \begin{cases} W_c\left(\dfrac{W_0}{W_c}h\right)^{1/m(T)} & (h \leqslant 0.96) \\ W_1 + 0.08\dfrac{W_2 - W_1}{h - 0.96} & (0.96 < h < 1.04) \\ W_c\left[0.037(h-1.04) + 0.3335\left(1 - \dfrac{T^2}{3.6\times 10^5}\right)\right] & (h \geqslant 1.04) \end{cases} \tag{34}$$

in which $m(T)$ is a coefficient dependent on temperature,

$$m(T) = 1.04 - \frac{(T+10)^2}{(T+10)^2 + 22.3(T_0+10)^2}. \tag{35}$$

A_d is calculated with the aid of the following equation:

Table 2. Parameter values utilized in the simulation

Parameters	Values	Parameters	Values
ρ	2200 kg m^{-3}	B_w	1.0×10^{-6} s m^{-1}
C	1100 J kg^{-1} K^{-1}	T_{en}	25°C
k	1.67 W m^{-1} K^{-1}	P_{en}	2850 N m^{-2}
C_w	4100 J kg^{-1} K^{-1}	W_c	300 kg m^{-3}
a_0	1.0×10^{-12} m s^{-1}	W_0	100 kg m^{-3}
B_r	1.0 W m^{-2} K^{-1}	T_0	25°C

$$A_d = \frac{\partial W_d}{\partial t} = \frac{\partial W_d}{\partial T}\frac{\partial T}{\partial t} \tag{36}$$

in which $\partial W_d/\partial T$ is obtained from the dehydration curve of Fig. 1 [4].

Computation of A_{vx} is as follows:

$$A_{vx} = \frac{a}{g} C_w \frac{\partial P}{\partial x} = \frac{a}{g} C_w \sum_{i=1}^{nen} \frac{\partial N_i}{\partial x} P_i(t). \tag{37}$$

The central difference scheme is employed for the calculation of $\partial W/\partial P$ and $\partial W/\partial T$.

$$\left(\frac{\partial W}{\partial P}\right)_{n+1} = \frac{W(P_{n+1}, T) - W(P_{n-1}, T)}{P_{n+1} - P_{n-1}} \tag{38}$$

$$\left(\frac{\partial W}{\partial T}\right)_{n+1} = \frac{W(P, T_{n+1}) - W(P, T_{n-1})}{T_{n+1} - T_{n-1}}. \tag{39}$$

Two-point linear elements are utilized for this one-dimensional problem. Twenty elements with a time step of 30 s are used and the convergence condition is selected to be TOL1 = 0.005 and TOL2 = 0.005 for all the computations.

Table 3. Time–temperature schedule

Temperature	Rate [°C h^{-1}]	Time [h]
25–200°C	30	5.83
200–200°C	0	10
200–625°C	30	14.17

For accuracy tests of the model, computations were carried out for case 4 using 40 elements with a time step of 15 s. It was found that the results were within 2% of those using 20 elements with a time step of 30 s.

For comparison, the same time–temperature schedule is used for all the computed cases. This schedule suggested by Gong *et al.* [6] is presented in Table 3.

Figures 2(a)–(d) and Figs. 3(a)–(d) demonstrate the evolution with time of the temperature and pore steam pressure distributions, respectively, of the four computed cases. It can be observed from these figures that there are no significant differences in the temperature distributions among the four cases, but the

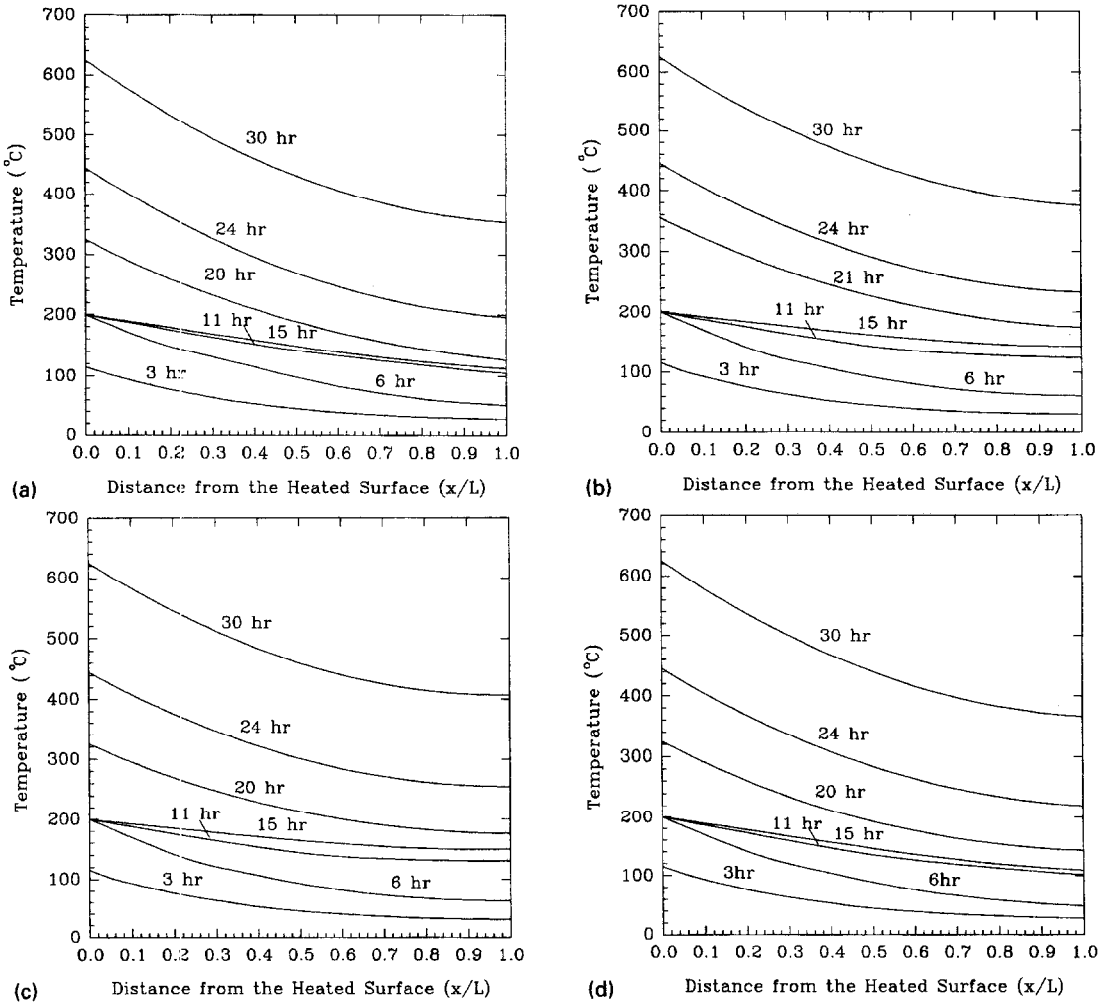

Fig. 2. Evolution of temperature distribution: (a) for case 1; (b) for case 2; (c) for case 3; (d) for case 4.

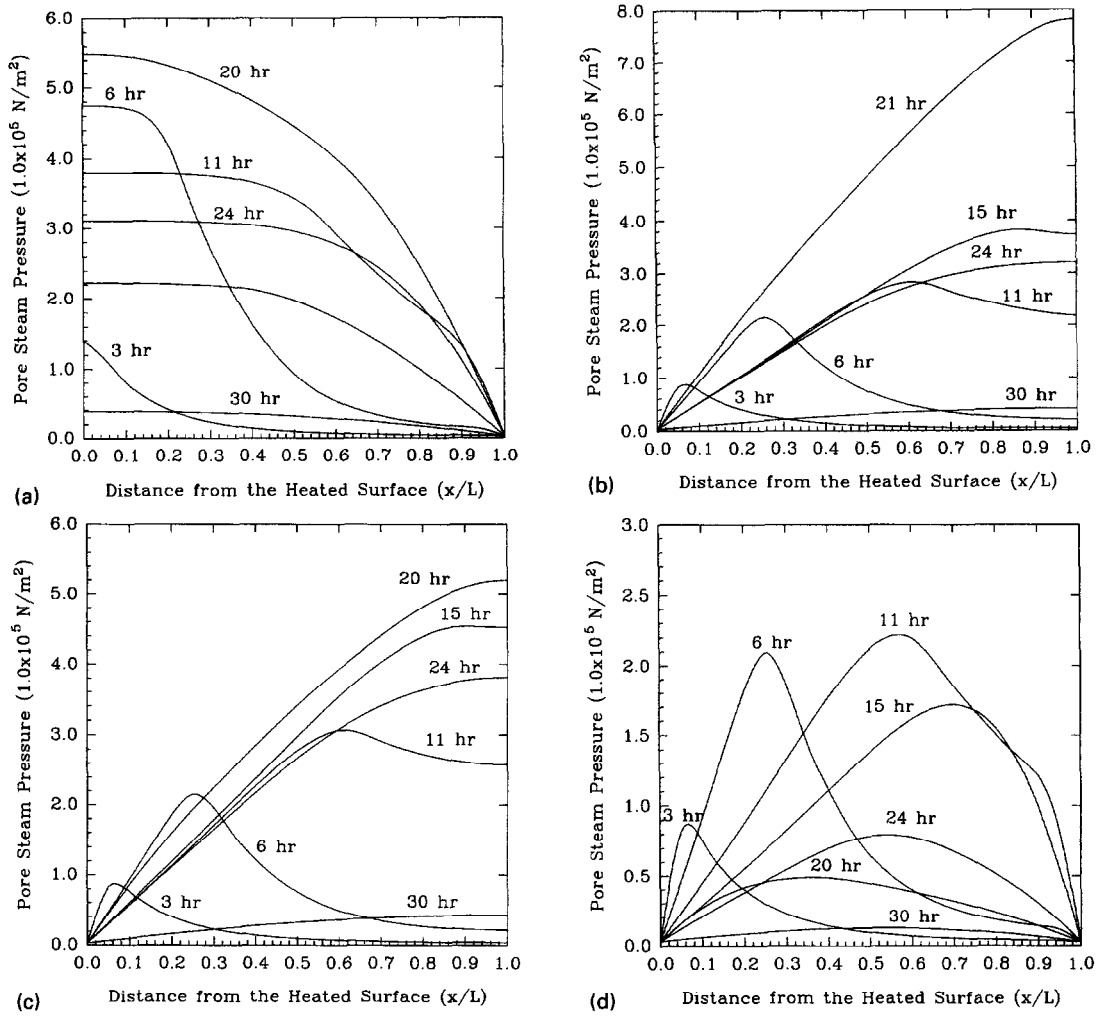

Fig. 3. Evolution of pore steam pressure distribution: (a) for case 1; (b) for case 2; (c) for case 3; (d) for case 4.

pore steam pressure distributions are very different except between cases 2 and 3. This is due to the difference in the pressure boundary condition. From Fig. 2(a)–(d) we can find that the temperatures of the unheated surface for the four cases are all around 400°C at the final stage of drying. The influence of radiation at the unheated surface has not been taken into account. This will be studied in a future paper.

Figure 4 compares the maximum pore steam pressure history curves for the four cases. Curves 1–4 are for cases 1–4, respectively. The predicted global maximum pore steam pressures are 5.69×10^5, 7.87×10^5, 5.30×10^5 and 2.33×10^5 N m^{-2} for cases 1–4, respectively. The global maximum pore steam pressures for cases 1 and 3 are over twice as great as that for case 4. The global maximum pore steam pressure for case 2 is over three times greater than that for case 4. From this comparison, it can be seen that an impermeable surface, whether the heated or the unheated, tends to develop higher pore steam pressures. This greatly increases the explosive tendency of

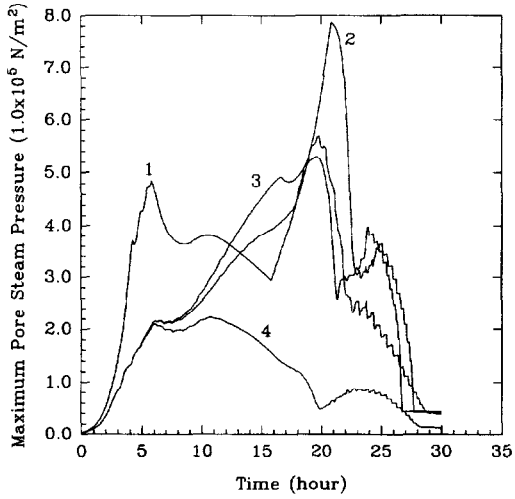

Fig. 4. Maximum pore steam pressure history curves.

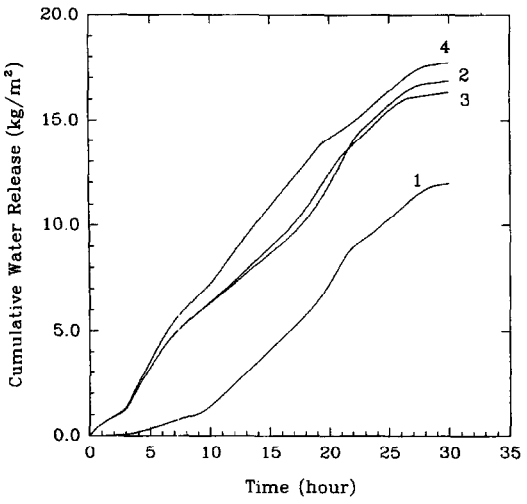

Fig. 5. Cumulative water release curves.

the concrete. Among the four cases, case 2 produces the highest pore steam pressure. This is caused by the heat loss at the unheated surface due to the convection heat transfer. The heat loss leads to a lower temperature at this surface, which slows down the development of a favourable pressure field for moisture transfer. (A favourable pressure field in this case should be that the pore steam pressure decreases from the impermeable unheated surface to the permeable heated surface.) Therefore, the moisture content close to the unheated surface is not decreased, but increased, at the earlier stage of the drying process. The increased moisture content naturally results in a higher pore steam pressure with the elevation of the temperature at the unheated surface.

The only way to lower the pressure for the first three cases is to increase the drying time. This is more energy-consuming and takes longer.

Figure 5 compares the cumulative water release curves for the four cases. Curves 1–4 correspond to cases 1–4, respectively. The predicted water release rate is much slower in case 1 than those in the other three cases. This is because a relatively high temperature is slow to set up and, therefore, so is a relative high pore steam pressure at the unheated surface (moisture transfer surface) in case 1. As a result, moisture transfer is much slower in the early stage of the drying process. The rates of moisture release in case 4 are the highest and the global maximum pore steam pressure is the lowest. This is due to the higher moisture transfer surface in this case.

An impermeable surface is extremely unfavourable to keep a low pore steam pressure and to moisture removal in the drying process. Therefore, an impermeable surface or one with low mass transfer rate should be avoided in the manufacturing process.

It is obvious that, when the boundary conditions of concrete installations are different, different time–temperature schedules need to be adopted for drying.

CONCLUDING REMARKS

A finite element model for the drying of refractory concrete is described. Simulations are carried out for concrete slabs to investigate the influence of an impermeable surface on pore steam pressure and moisture removal rates. Simulation results indicate that an impermeable surface can produce very high pore steam pressures in the drying process. This increases greatly the potential for explosive spalling. Experiments are required to validate the simulation results and enhance it for industrial application.

Acknowledgement—Z.-X. Gong gratefully acknowledges the financial support from McGill University in the form of a MCGILL/CIDA Fellowship. Also, the research support of Natural Sciences and Engineering Research Council and Exergex Corporation is sincerely appreciated.

REFERENCES

1. Z. P. Bazant and W. Thonguthai, Pore pressure and drying of concrete at high temperature, *Proceedings of the American Society of Civil Engineers*, Vol. 104, No. EM5, pp. 1059–1079 (1978).
2. Z. P. Bazant and W. Thonguthai, Pore pressure in heated concrete walls: theoretical prediction, *Mag. Concrete Res.* **31**(107), 67–76 (1979).
3. Z. P. Bazant, J. C. Chern and W. Thonguthai, Finite element program for moisture and heat transfer in heated concrete, *Nucl. Engng Des.* **68**, 61–70 (1981).
4. G. Dhatt, M. Jacquemier and C. Kadje, Modelling of drying refractory concrete. *Drying* '86 (Edited by A. S. Mujumdar), Vol. 1, pp. 94–104 (1986).
5. Z. X. Gong, B. Song and A. S. Mujumdar, Numerical simulation of drying of refractory concrete, *Drying Technol.* **9**, 479–500 (1991).
6. Z. X. Gong, G. S. Zhang and A. S. Mujumdar, Prediction of pore pressure of refractory concrete produced by firing, *Drying* '92 (Edited by A. S. Mujumdar), Part B, pp. 1780–1789 (1992).
7. Z. X. Gong and A. S. Mujumdar, A model for kiln-drying of refractory concrete, *Drying Technol.* **11**, 1617–1639 (1993).
8. Z. X. Gong and A. S. Mujumdar, A two-dimensional finite element model for kiln-drying of refractory concrete, *Drying Technol.* (in press) (1995).
9. O. C. Zienkiewicz, *The Finite Element Method.* McGraw-Hill, New York (1977).
10. T. J. R. Hughes, K. S. Pister and R. L. Taylor, Implicit–explicit finite elements in nonlinear transient analysis, *Comput. Meths Appl. Mech. Engrg* **17/18**, 159–182 (1979).
11. M. Song, Finite element analysis of heat and mass transfer in porous bodies, Masters Thesis (in Chinese), Tianjin Institute of Light Industry, China (1990).